Nanoscale Res Lett (2009) 4:431–436
DOI 10.1007/s11671-009-9270-5

NANO EXPRESS

Field Emission and Radial Distribution Function Studies of Fractal-like Amorphous Carbon Nanotips

F. Solá · A. Biaggi-Labiosa · L. F. Fonseca · O. Resto · M. Lebrón-Colón · M. A. Meador

Received: 30 September 2008 / Accepted: 28 January 2009 / Published online: 13 February 2009

Abstract The short-range order of individual fractal-like amorphous carbon nanotips was investigated by means of energy-filtered electron diffraction in a transmission electron microscope (TEM). The nanostructures were grown in porous silicon substrates in situ within the TEM by the electron beam-induced deposition method. The structure factor $S(k)$ and the reduced radial distribution function $G(r)$ were calculated. From these calculations a bond angle of 124° was obtained which suggests a distorted graphitic structure. Field emission was obtained from individual nanostructures using two micromanipulators with sub-nanometer positioning resolution. A theoretical three-stage model that accounts for the geometry of the nanostructures provides a value for the field enhancement factor close to the one obtained experimentally from the Fowler-Nordheim law.

Keywords Carbon nanotips · Graphite-like a-C · EELS · EFED · Field emission

Introduction

Nanotips made of carbon can have many different applications such as scanning microscope probes [1] and field emission (FE) sources [2]. For instance, recently carbon nanofibers were used as the electron source in order to test and build an FE display device prototype where a new nanocrystalline silicon—polymer film—was used as the phosphor material [3]. Carbon nanotubes, from single to film dispersed cases, have been extensively studied due to their tensile strength, electrical properties, chemical inertness, and high aspect ratio [4–10]. However, an advantage that amorphous carbon (a-C) nanotips have over carbon nanotubes is that when a-C nanotips are synthesized using the electron beam-induced deposition method with a transmission electron microscope (TEM-EBID) their growth process can be followed in real-time and the nanostructures can be grown at preferred positions by controlling the electron beam [11]. Recently, FE studies were done on an individual one-dimensional a-C nanotip grown by the TEM-EBID method, where a field enhancement factor of the order of 10 was found [12]. In this study, a field enhancement factor of the order of 10^3 was obtained for fractal-like a-C nanotips consisting of several branches, each branch similar in shape to the previously mentioned one-dimensional nanotips. A theoretical three-stage model that accounts for those findings is presented and discussed. Multistage models have been used for other types of nanostructures such as carbon nanotubes and tungsten oxide nanowires [7, 13–15]. In addition, we also present information of the short-range order of our nanostructures, using the radial distribution function (RDF) obtained by electron diffraction patterns. With this information average nearest-neighbor distances and their bond angle were obtained. The results are consistent with distorted graphitic-like structure that can account for the moderate conductivity of the tips observed in the FE results.

F. Solá · A. Biaggi-Labiosa · L. F. Fonseca (✉) · O. Resto
Department of Physics, Institute for Functional Nanomaterials, University of Puerto Rico, Rio Piedras, P.O. Box 23343, San Juan, PR 00931, USA
e-mail: luis.upr@gmail.com

M. Lebrón-Colón · M. A. Meador
Polymeric Materials Branch, Materials and Structures Division, National Aeronautics and Space Administration Glenn Research Center, 21000 Brookpark Road, Cleveland, OH 44135, USA

Experimental

The nanostructures were grown in situ in a TEM by the TEM-EBID method [11] using porous silicon (PSi) substrates. Full details about the PSi preparation procedure can be found elsewhere [16]. Pieces of the PSi films of the order of 2 mm^2 were attached to copper TEM grids. TEM-EBID experiments were made in a JEOL JEM-100S TEM at 100 kV. Electron energy loss spectroscopy (EELS) measurements were made in a Carl Zeiss LEO-922 TEM equipped with an Omega filter. Energy-filtered electron diffraction studies were done in a Phillips CM-200 TEM at 200 kV using a Gatan imaging filter. The energy selecting window used to filter the electron diffraction pattern was 10 eV and was centered at the zero loss peak of the electron energy loss spectrum. The inverse space was calibrated using a polycrystalline aluminum standard sample.

FE studies were done in an FEI Strata 235 Dual Beam FIB (DB-FIB) with a vacuum better than 10^{-5} Torr. Two electrochemically etched tungsten tips were connected to two Kleindiek micromanipulators, each having a positioning resolution of 0.25 nm. One of the tungsten tips is landed on a platinum contact which ends at the base of the nanostructure and the other is positioned close to the outer branches of the nanostructure to collect the FE current. The platinum contact was carefully deposited by SEM-EBID method using only the electron source of the DB-FIB. FE experiments were controlled with a LabView program and the beam was blanked before collecting the FE currents. Inspection of the samples after the FE measurements did not show additional growth of nanotrees.

Results and Discussion

A TEM image of fractal-like a-C nanotips is shown in Fig. 1. A qualitative growth mechanism for this type of nanostructure has been reported previously [17]. In a few words, the poor vacuum conditions in the JEOL JEM-100S TEM working without the liquid nitrogen trap brings hydrocarbon contamination inside the chamber which generally comes from the diffusion pump. Due to the incident electron beam, the hydrocarbon molecules are ionized. The high resistivity of the PSi samples allows the charging of the irradiated area, which becomes positively charged as secondary electrons leave the sample into the vacuum. Since there is no charge outside the sample, the Laplace equation is fulfilled. With these conditions, the hydrocarbons are attracted to the surface of the sample and preferentially deposited on hot spots with the highest local electric fields. Branching takes place during growth due to the preferential deposition near the tip regions. Finally, the deposited hydrocarbons are then transformed into a-C due to the continuous electron irradiation. With this technique, we recently developed methods to synthesize nanopalm-like silica/carbon heterostructures [16] and arrays of fractal-like a-C nanotips [11].

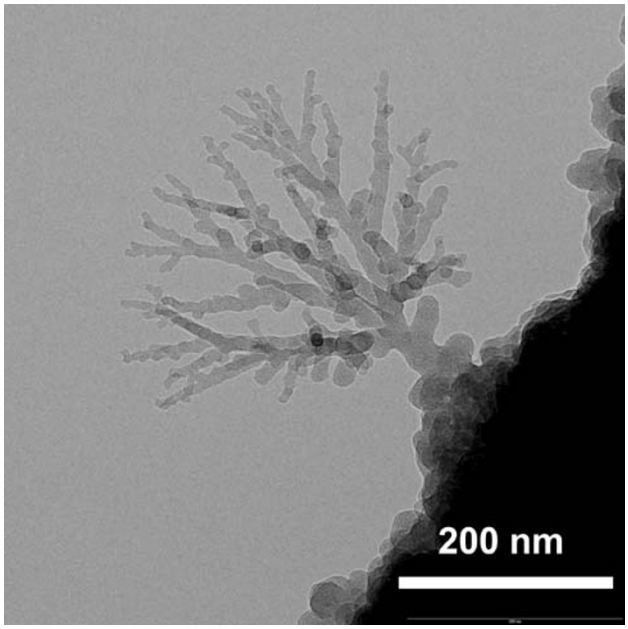

Fig. 1 TEM image of a fractal-like a-C nanotips obtained by TEM-EBID method

RDF Studies

Previous to the FE experiments we made energy-filtered convergent-beam electron diffraction (EFCBED) studies on the nanostructures to clarify the bonding and atomic order properties of the tips on which the FE properties will depend. Figure 2a is a low loss electron energy loss spectrum of fractal-like a-C nanotips. The first peak at 0 eV is the zero loss peak associated to the elastically scattered electrons. The second peak is located at 21.4 eV and it is related to the Plasmon energy (E_p) associated to the collective resonant oscillations of the valence electrons [18]. The Plasmon energy can be used to estimate the density of the nanostructures according to Eq. 1

$$p_0 = \frac{1}{4}\frac{M_C}{N_A} m * \frac{\varepsilon_0}{\hbar^2 e^2} E_p^2, \quad (1)$$

where $m^* = 0.87m$, m is the electron rest mass and the other factors have their usual meaning [19]. Taking the molar mass of carbon (M_C) as 12 g/mol, the density is found to be 1.44 g/cm^3, which is consistent with the density of graphite-like a-C [20]. The C–K energy-loss near-edge structure (ELNES) spectrum of the nanotips (Fig. 2b) exhibits two peaks. The first peak corresponds to a $1s \rightarrow \pi^*$ transition and the second peak to a $1s \rightarrow \sigma^*$

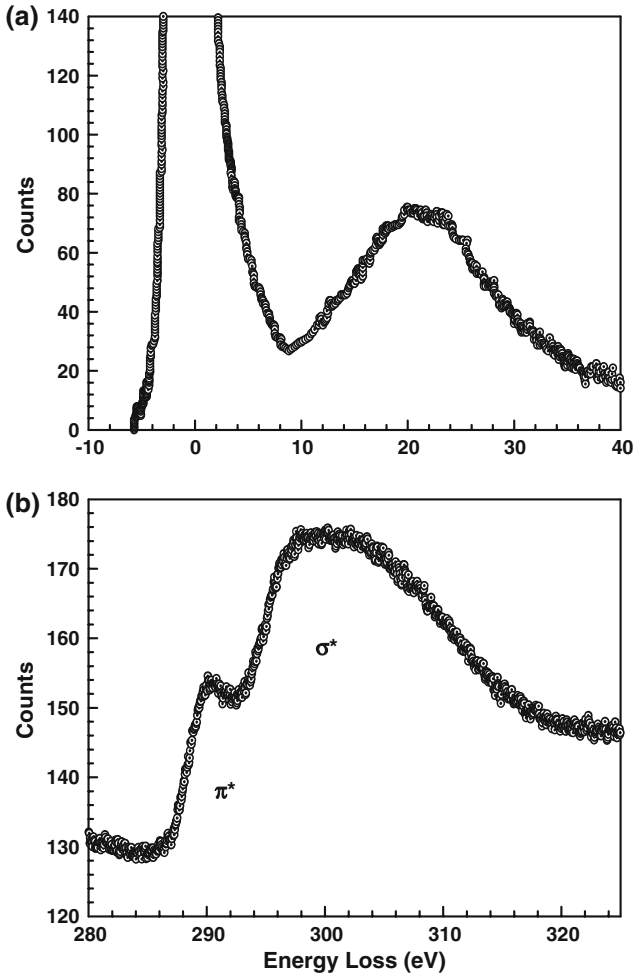

Fig. 2 **a** Low loss EELS showing the Plasmon energy at 21.4 eV. **b** C–K ELNES of a nanostructure typical of highly sp^2 amorphous carbon

transition. These two transitions are consistent with the ELNES spectrum of a-C [21]. Based on this type of spectrum we previously found a sp^2 bonding percentage around 80% for our nanostructures and when these results were compared with visible Raman studies, they were classified as graphite-like a-C with low hydrogen content [11].

Figure 3a shows the EFCBED pattern of fractal-like a-C nanotips. In order to avoid any damage to the CCD camera, the central spot of the EFCBED was positioned on the right corner. Cockayne and McKenzie [22] presented a pioneering study on calculating nearest-neighbor distances using EFED patterns. However, several improvements have been made to this study [23, 24]. Here we use the procedure presented in ref. [24] by splicing together two electron diffraction patterns with $\chi^2 = 0.0038$. First, the static structure factor was calculated. In Fig. 3b, we present the static structure factor $S(k)$ plot obtained using Eq. 2

$$S(k) = \frac{I(k)}{Nf^2(k)}, \tag{2}$$

where $I(k)$ is the azimuthally average intensity, $f(k)$ is the atomic scattering factor, N a fitting parameter, and $k = 2 \sin \theta/\lambda$ is the magnitude of the scattering vector. Secondly, the short-range order of individual fractal-like a-C nanotips can be investigated using the RDF defined as the probability to find an atom at a given distance from a particular atom. RDF is characterized by peaks from each shell of neighbors. The reduced RDF $G(r)$ is calculated by applying an inverse Fourier sine transformation to Eq. 3,

$$\Phi(k) = k[S(k) - 1] = \int_0^\infty G(r) \sin(kr) \mathrm{d}r, \tag{3}$$

where $\Phi(k)$ is the reduced intensity function, $G(r) = 4\pi r[p(r) - p_0]$ and $p(r)$ is the average density of neighbors a distance r from a particular atom. Figure 3c shows the reduced RDF $G(r)$ plot. At this point it is worth mentioning that the hydrogen contribution is excluded in p_0 because hydrogen is a weak scatterer and, hence, its contribution to the scattering intensity can be assumed to be negligible [25]. Taking first and second nearest-neighbor distances as the peak maxima of peaks 1 and 2 in the $G(r)$ plot, respectively, the values for r_1 and r_2 are: $r_1 = 1.49$ Å and $r_2 = 2.65$ Å. Furthermore, the average bond angle can be acquired using Eq. 4 [25]

$$\theta = 2 \sin^{-1}\left(\frac{r_2}{2r_1}\right). \tag{4}$$

From this expression, a bond angle of 124° was obtained. This bond angle differs from a sp^2 trigonally bonded carbon, which has a bond angle of 120°. This difference suggests that our nanostructures have a distorted graphitic structure which is consistent with our previous Raman and EELS results. From these findings it is expected that the a-C fractal nanotips will present good FE properties [26].

FE Studies

A SEM image of our FE set-up is shown in Fig. 4a, and the inset is the TEM image representative of the type of fractal nanotips tested. A typical FE current (I) curve is presented in Fig. 4b. For these measurements the distance (d) between the collection tip and the outer tips of the nanostructure was 252 nm. The turn on field was around 24 V/μm and is defined here as the field required for extracting a current of 10 nA, which is much lower than the 88 V/μm turn on field found in ref. [12] for a single nanotip. The fact that several branches are contributing to the total current can justify this difference. The inset of Fig. 4b is the corresponding Fowler-

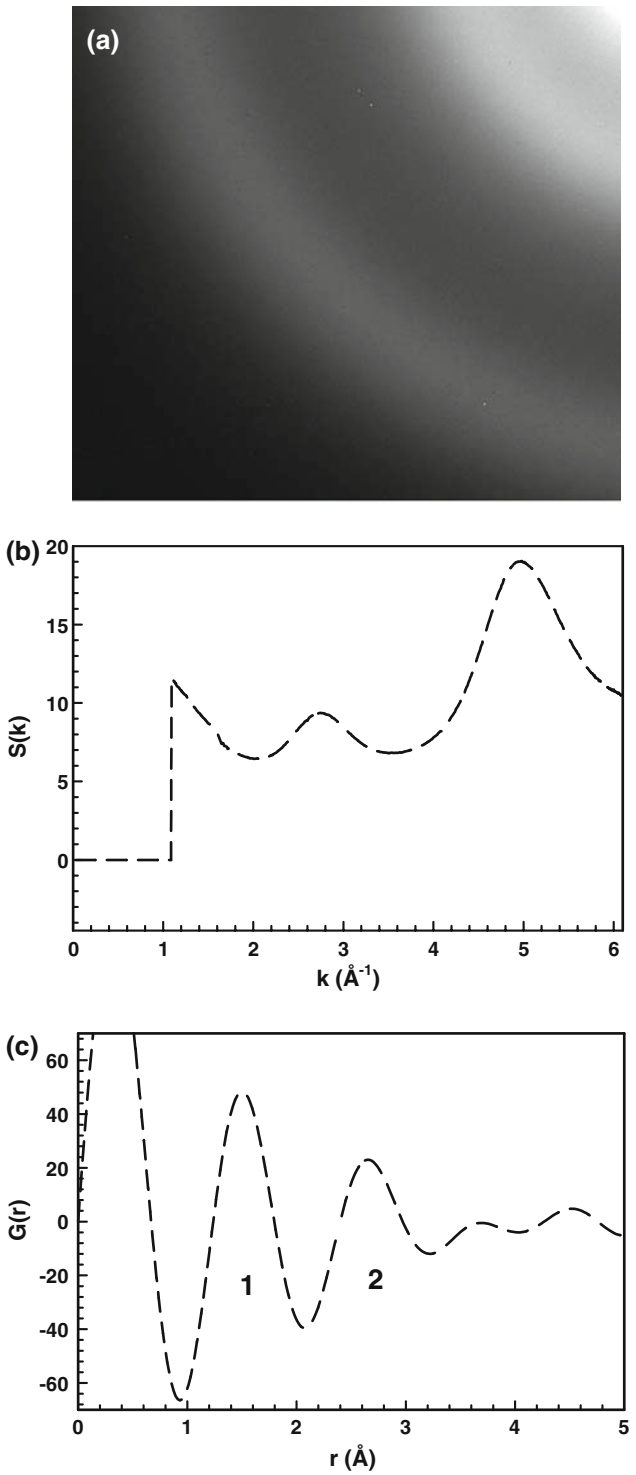

Fig. 3 **a** EFCBED pattern showing diffuse rings typical of an amorphous structure. The central spot is at the right corner. **b** Plot of the structure factor $S(k)$ with $k_{max} = 6$ Å^{-1}. **c** Corresponding reduced RDF plot of (**b**), where first and second nearest-neighbors distance peaks are marked 1 and 2, respectively

Nordheim (FN) plot ($\mathrm{Ln}(I/V^2)$ versus 1/V) which shows a fairly linear relation at low electric field intensities. At high electric fields the slope increases, which can be an indication of heating [2]. At the intermediate values of the electric field, the curve slightly deviates from the straight line. This deviation has been observed previously and explained in terms of the presence of adsorbates that enhances the tunneling probability [27]. In general, the curve suggests that the FE from the nanostructures follows the FN law expressed as

$$I = Aa\frac{E^2}{\phi}\exp\left(-b\frac{\phi^{3/2}}{E}\right), \tag{5}$$

where A is the emitting area (πr^2), E is the applied field, ϕ the work function of the material, and a and b are constants equal to 1.54×10^{-6} A eV V^{-2} and 6.83×10^3 eV$^{-3/2}$ V μm^{-1}, respectively [4]. Due to the tip-like geometry of our field emitters one can approximate E to $\beta V/d$, where β is the field enhancement factor that accounts for the geometry of the emitter. With this definition and rearranging Eq. 5, we can estimate β from the slope of the following relation

$$Ln\left(\frac{Id^2}{AV^2}\right) = \frac{-b\phi^{3/2}d}{\beta}\frac{1}{V} + Ln\left(\frac{a\beta^2}{\phi}\right) \tag{6}$$

Taking a work function of a graphitic structure of 5 eV [26], and the radius of the emitting area as $r \sim 0.5$ μm, the slope of Eq. 6 gives a β equal to 889. In trying to find a possible explanation of the previous enhancement factor, the multistage model [14] is used. We interpret the previous result of the field enhancement as a product of three stages. The schematic representation of our three-stage model is presented in Fig. 4c in which each stage represents an effective branch of the fractal-like a-C nanostructure. Each stage is defined with a particular length (l_i) and radius (r_i), where stage 1 has the biggest length and radius. In a multistage model the total enhancement factor can be written as a product of individual stages [7, 13–15]. With that interpretation β is written as

$$\beta = \beta_s \prod_{i=1}^{3} \beta_i, \tag{7}$$

where

$$\beta_i = \left(\frac{l_i}{l_i + d}\right)\left(1 + \frac{d}{r_i}\right) \text{ and } \beta_s = 1 - \exp\left[-a\left(\frac{s}{L}\right)\right]. \tag{8}$$

The expression for β_i was derived by Huang et al. [14]. The factor β_s is a factor that accounts for the screening effect of adjacent tips [28–30], where s is interpreted here as the average distance between adjacent tips, L is the sum of the lengths of three stages, and a is a fitting parameter [30]. Taking the common fitting parameter a equal to 2.3172 [28, 29], and measuring average values for l_i as 491 nm ($i = 1$), 146 nm ($i = 2$) and 74 nm ($i = 3$), average values of r_i as 13.4, 5.6, and 2.1 nm and with s

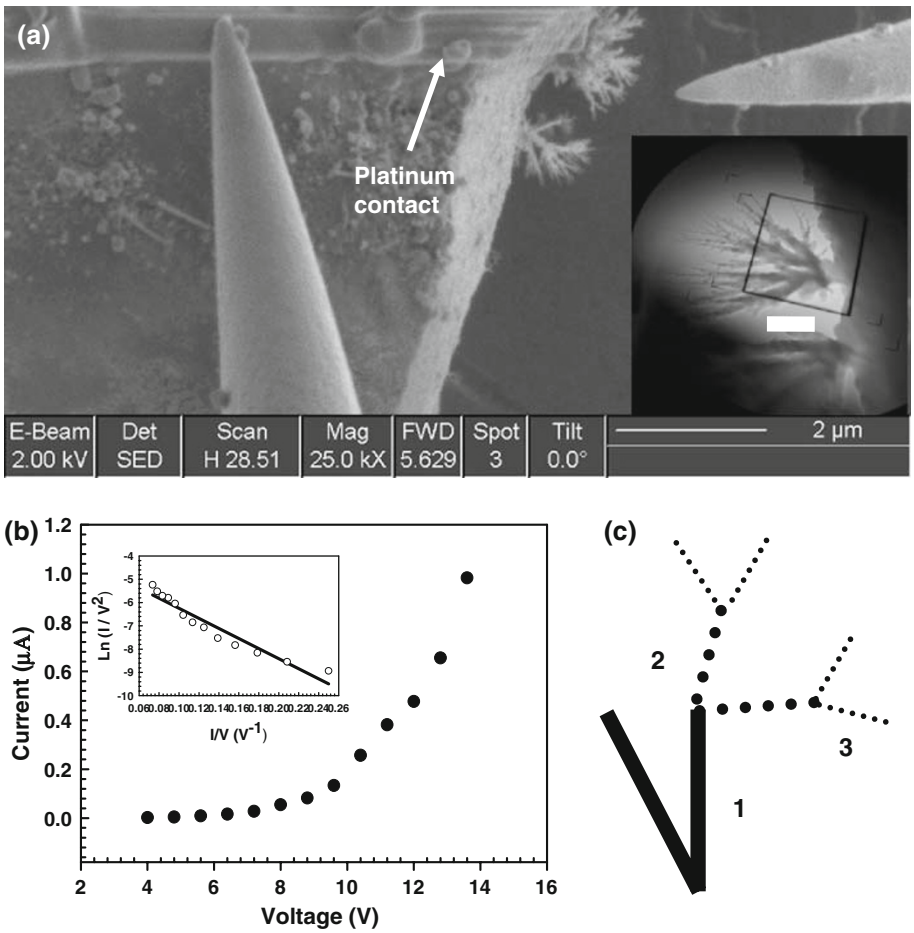

Fig. 4 **a** SEM image of our FE set-up. The inset is the TEM image representative of the type of fractal nanorods tested; the scale bar is 200 nm. **b** FE current curve obtained at a distance of 252 nm and the inset is the linear FN plot. **c** Schematic representation of the three-stage model. The *solid line* corresponds to the first stage and so on

equal to 54.7 nm, we obtain (from Eqs. 7 and 8) a field enhancement factor, β, equal to 981. This result agrees well with the value found experimentally of 889.

Conclusions

In summary, the reduced RDF analysis on the fractal-like a-C nanotips grown by the TEM-EBID method shows first and second bond lengths at 1.49 and 2.65 Å. Those nearest-neighbors distances defined an average bond angle of 124° which deviates from a trigonally sp^2 bonded carbon (120°) indicating a distorted graphite-like structure, which explains the moderate conductivity of the tips observed in the FE results. The electron FE measurements of the individual fractal-like a-C nanorods showed a turn on field of 24 V/μm. A three-stage model that accounts for the geometry of the nanostructures described well the value of the enhancement factor obtained experimentally from the FN law, and hence suggests a possible explanation of our observations. Hence, our observations show that these nanostructures are promising to be used in FE applications. In particular, the growth mechanism of the nanotrees' tips follows the path of maximum local field at the tips thus forming a nanostructure where the relationship between the density of tips and the local electric field intensity at the tips is optimized. It is worth to mention that for our calculations of the emission current densities we have used as the active emitting area the cross section of the total nanotree such that the values for the current density per branch's tip are lowest bound values.

Acknowledgments This study was supported by the following grants numbers and projects: NASA NNX08BA48A, NASA Space Grant NNG05GG78H, NSF 0701525, Fundamental Aeronautics Program and Subsonic Fixed Wing Project. The authors acknowledge the National Center for Electron Microscopy, Lawrence Berkeley Lab, which is supported by the U.S. Department of Energy under Contract #DE-AC02-05CH11231, and in particular to Dr. A. Minor for helping us with the FE experimental setup. F·S. kindly acknowledges Dr. D. J. H. Cockayne from Oxford University and D. Hull from NASA GRC for providing helpful information related to the electron diffraction analysis.

References

1. I.C. Chen, L.H. Chen, O. Christine, A. Quist, R. Lal, S. Jin, Nanotechnology **17**, 4322 (2006)
2. K.S. Yeong, B.C. Boothroyd, J.T.L. Thong, Nanotechnology **17**, 3655 (2006)

3. A. Biaggi-Labiosa, F. Solá, O. Resto, L.F. Fonseca, A. González-Berríos, J. De Jesús, G. Morell, Nanotechnology **19**, 225202 (2008)
4. M. Passacantando, F. Bussolotti, S. Santucci, A. Di Bartolomeo, F. Giubileo, L. Iemmo, A.M. Cucolo, Nanotechnology **19**, 395701 (2008)
5. X.J. Li, W.F. Jiang, Nanotechnology **18**, 065203 (2007)
6. Z. Xu, X.D. Bai, E.G. Wang, Z.L. Wang, Appl. Phys. Lett. **87**, 163106 (2005)
7. D.L. Niemann, B.P. Ribaya, N. Gunther, M. Rahman, J. Leung, V. Nguyen, Nanotechnology **18**, 485702 (2007)
8. R.C. Smith, D.C. Cox, S.R.P. Silva, Appl. Phys. Lett. **87**, 103112 (2005)
9. S.H. Jo, Y. Tu, Z.P. Huang, D.L. Carnahan, D.Z. Wang, Z.F. Reng, Appl. Phys. Lett. **82**, 3520 (2003)
10. J.M. Bonard, K.A. Dean, B.F. Coll, C. Klinke, Phys. Rev. Lett. **89**, 1976021 (2002). doi:10.1103/PhysRevLett.89.197602
11. F. Solá, O. Resto, A. Biaggi-Labiosa, L.F. Fonseca, Micron **40**, 80 (2009)
12. C.H. Jin, J.Y. Wang, Q. Chen, L.M. Peng, J. Phys. Chem. B **110**, 5423 (2006). doi:10.1021/jp057240r
13. R. Seelaboyina, S. Boddepalli, K. Noh, M. Jeon, W. Choi, Nanotechnology **19**, 065605 (2008)
14. J.Y. Huang, K. Kempa, S.H. Jo, S. Chen, Z.F. Ren, Appl. Phys. Lett. **87**, 053110 (2005)
15. R. Seelaboyina, J. Huang, J. Park, D.H. Kang, W.B. Choi, Nanotechnology **17**, 4840 (2006)
16. F. Solá, O. Resto, A. Biaggi-Labiosa, L.F. Fonseca, Nanotechnology **18**, 405308 (2007)
17. F. Banhart, Phys. Rev. E **52**, 5156 (1995)
18. R.F. Egerton, *Electron Energy Loss Spectroscopy in the Electron Microscope* (Plenum Press, New York, 1996), Chapter 3
19. A.C. Ferrari, A. Libassi, B.K. Tanner, V. Stolojan, J. Yuan, L.M. Brown, S.E. Rodil, B. Kleinsorge, J. Robertson, Phys. Rev. B **62**, 11089 (2000). doi:10.1103/PhysRevB.62.11089
20. S.R.P. Silva, *Properties of Amorphous Carbon* (Inspec, London, UK, 2003), Chapter 1
21. K. Uppireddi, O. Resto, B.R. Weiner, G. Morell, Nanoscale Res. Lett. **3**, 65 (2008)
22. D.J.H. Cockayne, D.R. McKenzie, Acta Crystallogr. A **44**, 870 (1988)
23. W. McBride, D.J.H. Cockayne, J. Non-Cryst. Solids **318**, 233 (2003). doi:10.1016/S0022-3093(02)01908-7
24. T.C. Petersen, W. McBride, D.G. McCulloch, I.K. Snook, I. Yarovsky, Ultramicroscopy **103**, 275 (2005)
25. R.D. Evans, J. Bentley, K.L. More, G.L. Doll, J.T. Glass, J. Appl. Phys. **96**, 273 (2004). doi:10.1063/1.1760232
26. A.C. Ferrari, B.S. Satyanarayana, J. Robertson, W.I. Milne, E. Barborini, P. Piseri, P. Milani, Europhys. Lett. **46**, 245 (1999)
27. K.S. Yeong, J.T.L. Thong, Appl. Surf. Sci. **233**, 20 (2004). doi:10.1016/j.apsusc.2004.03.222
28. J. Xiao, X. Zhang, G. Zhang, Nanotechnology **19**, 295706 (2008)
29. Y.W. Zhu, T. Yu, F.C. Cheong, X.J. Xu, C.T. Lim, V.B.C. Tan, J.T.L. Thong, C.H. Sow, Nanotechnology **16**, 88 (2005)
30. X. Qian, H. Liu, Y. Guo, Y. Song, Y. Li, Nanoscale Res. Lett. **3**, 303 (2008)